Li et al. *NPG Asia Materials* (2018) 10: 238–254
DOI 10.1038/s41427-018-0027-4

NPG Asia Materials

ARTICLE Open Access

Amphiphilic dendrimer engineered nanocarrier systems for co-delivery of siRNA and paclitaxel to matrix metalloproteinase-rich tumors for synergistic therapy

Xin Li[1], A-ning Sun[1], Yu-jie Liu[1], Wen-jie Zhang[1], Ning Pang[1], Shi-xuan Cheng[1] and Xian-rong Qi[1]

Abstract

Combinations of chemotherapeutics with small interfering RNA (siRNA) can incorporate the advantages of their different mechanisms to exert a synergetic effect. A safe and effective vehicle for simultaneous delivery of the components to tumor cells is a prerequisite for obtaining the optimum effect. We developed an amphiphilic dendrimer engineered nanocarrier system (ADENS) for co-delivering paclitaxel and siRNA for cancer treatment. This nanocarrier possesses a unique hollow core/shell structure in which siRNA is incorporated in the hydrophilic cavity and large quantities of paclitaxel are stored in the hydrophobic interlayer, while the outer PEG layer serves to prolong the circulation time. Further modification by tumor microenvironment-sensitive polypeptides (TMSP) significantly enhanced the cellular uptake, tumor penetration and tumor accumulation of the ADENS by a tumor microenvironment-triggered mechanism. TMSP-ADENS had prominent therapeutic effects at a relatively low drug dose both in vitro and in vivo. In A375 xenograft mice, TMSP-ADENS/siRNA/PTX showed the highest VEGF mRNA inhibition rate of 73% and suppressed tumor growth and relapse, while Taxol did not show an effect on tumor relapse. The anti-tumor and anti-angiogenic effects were further confirmed in an HT-1080 xenograft tumor model. Our findings, combined with the known biodegradability and tunable physicochemical properties of these polymers, suggest that this TMSP-ADENS can be a robust co-delivery system for cancer combination therapy in the future.

Introduction

Single drug therapy shows certain limitations in treating cancers, as the multiple genetic changes, complexity of cancer progression mechanisms and heterogeneity of the tumor microenvironment pose a complex challenge for anticancer drugs[1–3]. Multidrug resistance (MDR) and the high systemic toxicity of drugs are also insurmountable challenges[4]. Thus, combination therapies of two or more agents aimed at different targets or acting by different anticancer mechanisms have been explored as a promising strategy due to the potent additive or synergistic anticancer activity as well as the moderate toxicity and MDR[5–8]. Among the various drug combinations, small interfering RNA (siRNA) and chemotherapeutic drugs have been a focus of attention in recent years[4]. siRNA can specifically silence the target gene without exerting toxicity on normal cells and has excellent prospects in treating a range of diseases[9]. However, the instability, polyanionic macromolecular characteristics and poor cellular uptake of siRNA remain major hurdles in its systemic administration. Considerable efforts have been made to facilitate siRNA delivery, among

Correspondence: Xian-rong Qi (qixr@bjmu.edu.cn)
[1]Beijing Key Laboratory of Molecular Pharmaceutics and New Drug Delivery System, School of Pharmaceutical Sciences, Peking University, Beijing 100191, PR China
These authors contributed equally: Xin Li, A-ning Sun.

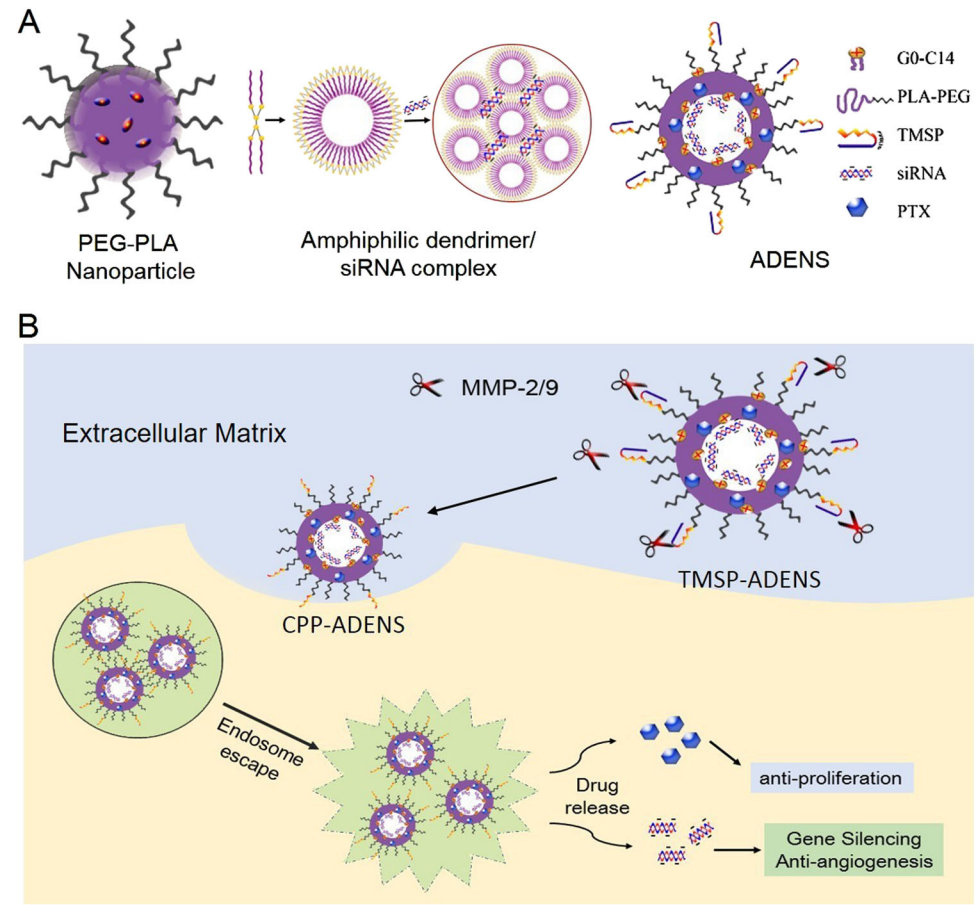

Fig. 1 a Schematic structure of typical PEG-PLA nanoparticles with drugs in the PLA core (left), an amphiphilic dendrimersome and its complex with siRNA (middle), and the three layer structure of the ADENS (right). **b** Representation of the MMP-2/9 response, internalization and intracellular transportation of TMSP-ADENS. The simultaneous delivery of siRNA and PTX in tumor cells is the basis for the optimal therapeutic efficacy of the combination strategy of siVEGF for anti-angiogenesis and PTX for cytotoxicity

which nanotechnology offers a potential solution for addressing the problem. Ideal siRNA delivery vehicles should be engineered from biocompatible materials and should be able to effectively entrap siRNA, facilitate its cellular uptake and improve its pharmacological properties by protecting it from serum nucleases, renal filtration, and uptake by the mononuclear phagocyte system[10,11]. Cationic lipids and polymers, two major non-viral vehicles, can assemble with siRNAs to form nanoscale complexes through electrostatic interactions and deliver siRNA from circulation into cells[12]. However, nanoparticles that are polycation-nucleic acid composites or normal cationic liposomes are known to be unstable in biological fluids such as blood[13,14]. The fabrication of nanocarriers that can efficiently co-encapsulate siRNA and chemotherapeutics to simultaneously deliver the two or more components to tumor cells represents an even steeper requirement.

The poly(ethylene glycol)-block-poly (D,L-lactic acid) (PEG-PLA) block copolymer is a widely used and reliable biodegradable polymer that has been approved by the Food and Drug Administration (FDA) for multiple drug delivery and biomedical device applications[15]. PEG-PLA can self-assemble into nanoparticles via various preparation methods. The nanoparticles composed of PEG-PLA have high loading efficiency for a wide range of hydrophobic drugs and exhibit sustained release through polymer degradation and drug diffusion[16–18]. There has been an approved product based on PEG-PLA micelles in South Korea for the poorly water-soluble drug paclitaxel (PTX)[19,20]. However, the previous formulations are designed for delivery of a single chemotherapeutic drug and are not entirely appropriate for use in the co-delivery of siRNA molecules. Considering the hydrophilicity and electronegativity of siRNA, additional compartment space and cationic components are required for such a co-delivery system. Therefore, we constructed a cationic Amphiphilic Dendrimer Engineered Nanocarrier System (ADENS)

co-encapsulating siRNA and PTX with PEG-PLA and an amphiphilic dendrimer (G0–C14) by a simple double emulsion-solvent evaporation technique. In contrast, the lipid hybrid nanoparticles formed by polymers and lipids or lipids-PEG are described as a polymeric core coated with single or multiple layers of lipids constituting the shell[21–23]. The structure of the ADENS was proved to be a unique hollow core/shell structure, as illustrated in Fig. 1a, including (i) an aqueous hollow core encapsulating hydrophilic and electronegative siRNA, (ii) a middle layer of PLA and alkyl chains surrounding the aqueous core and accommodating the hydrophobic drug PTX, and (iii) an outer PEG layer that provides a relatively neutral surface charge and stealth coating, enabling the nanocarriers to avoid being captured by the reticuloendothelial system and to prolong their in vivo circulation time. This structure is capable of encapsulating both hydrophobic and hydrophilic substances in different compartments and exhibiting high structural integrity, stability during storage, controlled release, and high biocompatibility. Appealingly, the siRNA molecules are entrapped in the inner core of ADENS, which we believe could provide better protection than just absorbing them on the surface[13].

Overexpressed MMP is a major hallmark of the tumor microenvironment in a wide range of cancer types and is associated with tumor progression, angiogenesis, invasion and metastasis. To improve tumor delivery, enhance penetration specificity and minimize off-target effects, we modified the ADENS by tumor microenvironment-sensitive polypeptides (TMSP), which are composed of the cell-penetrating peptides (CPP, oligoarginine) and shielding peptides (EGGEGGEGGEGG) connected by a matrix metalloproteinases-2/9 (MMP-2/9)-cleavable peptide linker (PVGLIG)[24,25]. The TMSP-ADENS would remain unrecognized by normal cells to nullify the non-selectivity of CPP. When they reached the tumor and responded to the MMP stimuli, the exposed CPP would promote cellular uptake[24–30]. As shown in Fig. 1b, MMP-2/9 functions as a "scissor" to cleave the shielding group of TMSP by hydrolyzing the PVGLIG linker. Then, the exposed CPP would facilitate the cell penetration of the nanocarriers. After being uptaken by cells, the nanocarriers were first distributed in endosomes and then escaped from the endosomes and entered the cytoplasm. The drugs were released to reach their respective targets and exerted their effects. The stimuli-response uptake strategy has been proven in our previous works to be a promising method for tumor-targeting therapy[24,25,28–30]. TMSP-modified nanoparticles or prodrugs have been revealed as a robust drug delivery system, showing enhanced accumulation and deeper penetration into tumors and mediating significant anti-tumor effects with moderate toxicity to normal cells and tissues.

Materials and methods

Materials

Maleimide-PEG_{4000} was purchased from Jenkem Technology Co., Ltd. (Beijing, China). Methoxy-PEG_{4000} and 1,2-epoxytetradecane were purchased from TCI (Tokyo, Japan), and generation 0 of the polyamidoamine (G0-PAMAM) dendrimer was purchased from Sigma-Aldrich (St. Louis, USA). D,L-lactide was provided from Alfa Aesar (Ward Hill, UK). Tumor microenvironment-sensitive peptides ($(EGG)_4$-PVGLIG-r_9-C) and cell penetration peptide (r_9) were synthesized via a standard Fmoc solid-phase peptide synthesis method by China Peptides Co., Ltd. (Shanghai, China). Paclitaxel (PTX) was purchased from Norzer Pharmaceutical Co., Ltd. (Beijing, China), and Taxol was from Bristol-Myers (New York, USA). The scrambled siRNA (siN.C, antisense strand, 5'-ACGUGACACGUUCGGAGAATT-3'), FAM-labeled siRNA (FAM-siRNA) and VEGF siRNA (siVEGF, antisense strand, 5'-GAUCUCAUCAGGGUACUCCdTdT-3') were purchased from Genepharma (Suzhou, China). The siRNAs are double-stranded RNA oligos containing 21 NT. All primers were synthesized by Generay Biotech (Shanghai, China). 3-(4,5-Dimethylthiazol-2-yl)-2,5-diphenyltetrazolium bromide (MTT), 6-coumarin (COU, purity >99%) and collagenase IV were purchased from Sigma-Aldrich (St. Louis, USA). GM6001 was purchased from HARVEY (Beijing, China). The A375, PC-3 and HT-1080 cell lines originated from American Type Culture Collection. Fetal bovine serum (FBS) was obtained from Gibco (Grand Island, USA). RPMI-1640 medium, modified Eagle's medium (MEM), DMEM, penicillin-streptomycin, trypsin and Hoechst 33258 were obtained from Macgene Technology (Beijing, China). LysoTracker Red was purchased from Invitrogen (Carlsbad, USA).4-aminophenylmercuric acetate (APMA) was purchased from Merck Co, Ltd, (Darmstadt, Germany).

Male BALB/c nu/nu mice (18–20 g) were purchased from Beijing Vital River (Beijing, China), and all of the animals were kept in standard housing conditions (SPF) with free access to standard food and water. All the animal experiments were performed in compliance with the relevant laws and institutional guidelines of the Institutional Animal Care and Use Committee of Peking University Health Science Center and were approved by the Institutional Animal Care and Use Committee of Peking University Health Science Center (Beijing, China).

Synthesis of copolymers and amphiphilic dendrimer

Methoxy-PEG-PLA and maleimide-PEG-PLA copolymers were synthesized by ring-opening polymerization. Briefly, purified D,L-lactide was combined with either MeO-PEG or Mal-PEG (6:1, w/w) in anhydrous toluene, and 0.01% stannous octoate was added as a catalyst. The reaction was carried out under a moisture-free argon

atmosphere at 110°C for 24 h. The product was collected and purified by dissolution and precipitation and dried in vacuum. TMSP were conjugated to Mal-PEG-PLA using the previously reported method by stirring in dimethylformamide (DMF) containing triethylamine (TEA)[23]. G0–C14 was synthesized by Michael addition chemistry between 1,2-epoxytetradecane and the free amines on G0-PAMAM according to a reported procedure[31]. The mixture of 1,2-epoxytetradecane and PAMAM dendrimer (6:1, mol/mol) was vigorously stirred at 90 °C for 2 days. The crude yellow product was separated by chromatography on silica and eluted from CH_2Cl_2 to 75:22:3 CH_2Cl_2/MeOH/NH_4OH. The separated product was characterized by chromatography and ^1H NMR. As calculated from ^1H NMR, the molecular weight of the PLA block was ~18,000.

Preparation of ADENS

The ADENS co-encapsulating siRNA and PTX was formulated via the double emulsion-solvent evaporation method[22]. First, 200 µl of siRNA solution (0.1% DEPC-treated water) was dropped into 0.5 mL of chloroform containing PEG-PLA, G0–C14 and PTX, and then the mixture was emulsified by probe sonication (80 w, 30 s) to form the primary emulsion. Next, the primary emulsion was dispersed into 3 mL of 0.5% (w/v) PVA aqueous solution and further emulsified by probe sonication (100 w, 2 min), resulting in the formation of the double emulsion. The remaining organic solvent was removed by rotary evaporation. TMSP-ADENS was prepared by the same procedure except that 5% (mol ratio) TMSP-PEG-PLA was mixed in PLA-PEG. FAM-siRNA and lipophilic fluorescent dyes were used to replace siRNA and PTX to prepare the fluorescently labeled ADENS.

Determination of PTX Loading

The amount of PTX encapsulated in ADENS was determined by high-performance liquid chromatography (HPLC, LC-20AT Pump, SPD-20A UV detector, Shimadzu, Kyoto, Japan) equipped with an RP-18 column (4.6 × 250 mm, pore size 5 µm, Diamonsil, Beijing, China). The assay was conducted with a mobile phase composed of acetonitrile: distilled water (55:45, v/v) at a flow rate of 1 mL/min and an ultraviolet detector operating at a wavelength of 227 nm.

Determination of siRNA loading and stability

To determine the siRNA complexation ability at various G0–C14/siRNA weight ratios, agarose gel electrophoresis was conducted with the final siRNA concentration fixed at 1 µM. The complexes were added with loading buffer on a 1% agarose gel containing 0.5 µg/mL ethidium bromide. Electrophoresis was performed at 100 mV for 10 min in TBE buffer (40 mM Tris, 1 mM EDTA, pH 8), and then the gels were photographed under UV illumination. Free siRNA was used as the control. siRNA stability in serum was determined by individually mixing free siRNA, G0–C14/siRNA, ADENS/siRNA and PEI/siRNA with FBS (1:1, v/v) at 37 °C. Aliquots taken at the indicated time intervals were measured by 1% agarose gel electrophoresis.

In vitro release of PTX and siRNA

The PTX release from the ADENS loaded with 0.6 mg of PTX was determined by suspending it in dialysis bags with a cut off M.W. of 7000 Da. Then, the dialysis bags were put into 40 mL of phosphate-buffered saline (PBS) as the release medium at 37 °C and shaken at 100 r.p.m. At specific intervals, 1 mL of the incubation medium was drawn, and the same volume of fresh solution was added. The amount of PTX released at each time point was determined by an HPLC assay as described above.

The siRNA release from the ADENS was conducted in PBS at 37 °C. The ADENS containing FAM-siRNA was dissolved in PBS at 37 °C. 500 µL of the samples were taken out at certain time points, centrifuged (20,000×*g*) for 15 min, and the supernatant containing free FAM-siRNA was collected. The FAM-siRNA concentration was determined by a fluorescence spectrophotometer at Ex/Em = 484/525 nm.

Characterization of the ADENS

The size, polydispersity index (PDI) and zeta potential of the ADENS were determined by dynamic light scattering (DLS) using a Malvern Zetasizer Nano ZS (Malvern, UK). The morphology of the ADENS was observed by transmission electron microscopy (TEM, JEM 1400-Plus, JEOL, Tokyo, Japan) after negative staining with phosphotungstic acid (2%). The interaction between siRNA and the hydrophobic polymer components during the emulsification process was investigated by using DiD to label the oil phase, and the locality of FAM-siRNA in the primary emulsion was visualized by Leica SP8 confocal laser scanning microscopy (CLSM, Leica Microsystems, Heidelberg, Germany).

Förster resonance energy transfer (FRET) experiments

DiO (Ex/Em = 484/501 nm) and DiI (Ex/Em = 549/566 nm) co-loaded hybrid nanocarriers, DiO-loaded PEG-PLA nanoparticles and DiI-loaded G0–C14 nanoparticles were prepared. Then, the co-loaded ADENS, mixture of DiO/PEG-PLA nanoparticles and DiI/G0–C14 nanoparticles, and DiO/PEG-PLA nanoparticles alone were excited at 484 nm to obtain the FRET spectra[32].

Cellular Uptake

The cellular uptake of the ADENS and TMSP-ADENS loaded with FAM-siRNA by HT-1080, A375 and PC-3

cells was detected by flow cytometry. Cells seeded in 6-well plates (Corning, USA) were incubated with serum-free medium containing free FAM-siRNA, ADENS/FAM-siRNA, or TMSP-ADENS/FAM-siRNA at equivalent FAM-siRNA concentrations for 4 h. Then, the cells were collected, washed, suspended in PBS and analyzed by FACSCalibur (Becton Dickinson, San Jose, USA). To study the influence of the MMP-2/9 level on cellular uptake, the HT-1080 cells were pre-incubated with various concentrations of activated collagenase IV or 100 mM GM6001 (an MMP inhibitor) for 1 h. Then, TMSP-ADENS/COU was added and incubated for another 2 h. The cells were analyzed by FACSCalibur with the procedure described previously. Collagenase IV containing MMP-2 and MMP-9 was first activated by 2.5 mM APMA solution at 37°C for 2 h[24,33].

Intracellular Trafficking and Endosome Escape

HT-1080 cells were seeded in confocal dishes at 2×10^5 cells per well. After 24 h of incubation, the ADENS and TMSP-ADENS loaded with both FAM-siRNA and Nile Red were added into each dish for 4 h in serum-free MEM. After 4 h of incubation, the cells were washed with PBS three times and fixed with 4% paraformaldehyde for 15 min at room temperature. The cell nuclei were stained with Hoechst 33258 (5 μg/mL). The cells were observed and imaged with a Leica SP8 confocal microscope. To track the endosomal escape of siRNA, HT-1080 and A375 cells were incubated for 2 h, 4 h and 8 h with TMSP-ADENS/FAM-siRNA (100 nM). At each time interval, LysoTracker Red (150 nM) was added to the medium and incubated with the cells for 30 min at 37°C for endosome/lysosome labeling. The cells were imaged by CLSM.

Antiproliferation Measurement

The antiproliferative effect was evaluated by the MTT assay. Cells were seeded in 96-well plates at a density of 5000 cells/well. Various formulations at a range of drug concentrations were given to the cells in the exponential growth phase for 48 h. Then, 20 μL of MTT (5 mg/mL in PBS) was added to each well. After incubation for 4 h, the medium was removed, and DMSO was added to dissolve the formazan. The absorbance was measured by an iMark microplate reader (Bio-Rad, Hercules, CA, USA) at a wavelength of 570 nm.

In vitro siRNA transfection

A375 cells were transfected with TMSP-ADENS/siVEGF, ADENS/siVEGF and TMSP-ADENS/siN.C at a siRNA concentration of 100 nM. The cell medium was collected, and the amount of secreted VEGF in the supernatant medium was quantified by a human VEGF enzyme-linked immunosorbent assay (ELISA) kit (eBioscience, San Diego, USA) according to the manufacturer's protocol. The VEGF mRNA was evaluated by quantitative real-time polymerase chain reaction (qRT–PCR), and the siRNA concentration in these treatment groups was 50 nM. Cells were collected, and total RNA was extracted using TRNzol A^+ reagent (Tiangen, Beijing, China) and then reverse transcribed with a reverse transcription kit (Promega, Madison, USA). The resulting cDNAs were used for RT-PCR analysis with VEGF as the targeting gene and GAPDH as the housekeeping gene. This was carried out with GoTaq qPCR Master Mix from Promega in triplicate. The PCR procedure was performed on an IQ5 real-time PCR detection system (Bio-Rad, Hercules, USA), and the relative VEGF gene expression was calculated by the ΔΔCt method.

ADENS biodistribution in the xenograft model

HT1080 human fibrosarcoma cells suspended in DMEM (5×10^7/mL) were inoculated subcutaneously in the right armpit of female BALB/c nu/nu mice. The tumor volumes were approximately 500 mm^3 (~10 days after inoculation). ADENS/Cy5-siRNA and TMSP-ADENS/Cy5-siRNA (Cy5-siRNA = 670 μg/kg) were injected via the tail vein ($n = 3$). In addition, one mouse injected with 5% glucose solution served as a control. Mice were anesthetized with 3% isoflurane gas at 1, 3, 6, 11, and 24 h after injection, and fluorescent images were taken and analyzed with a Maestro Automated In Vivo Imaging system (CRI, Inc., Woburn, USA). The excitation wavelength was 630 nm, and the detection wavelength was 700 nm. The mean fluorescence intensity is defined as the average photon count per unit area of tumor.

Intratumoral Accumulation of ADENS

The intratumoral distributions of DiD-loaded ADENS and TMSP-ADENS were analyzed by CLSM (Ex/Em = 644/665 nm). BALB/c nu/nu mice bearing HT-1080 tumors (the tumor volume was ~500 mm^3) were divided into two groups and administered either ADENS/DiD or TMSP-ADENS/DiD (DiD = 80 μg/kg) by i.v. injection. At 24 h after the injection, the tumors were isolated and fixed in 4% formaldehyde overnight at 4°C. Subsequently, the fixed tumor tissues were sectioned and counterstained with Hoechst 33258 and imaged with a confocal microscope.

Tumor Inhibition in Xenograft Tumor Models

We developed a tumorigenesis-relapse model of A375 cell-xenografted mice to assess anticancer effects. A375 cells were injected subcutaneously in the right armpit of BALB/c nu/nu mice. During the early stage of tumorigenesis, when the tumor volume reached ~100 mm^3, the mice were randomly divided into six groups ($n = 6$), and 1 mg/kg siVEGF and 3 mg/kg PTX were given simultaneously or alone in the above forms via i.v. at Day 0 and Day 2 (the day of the first

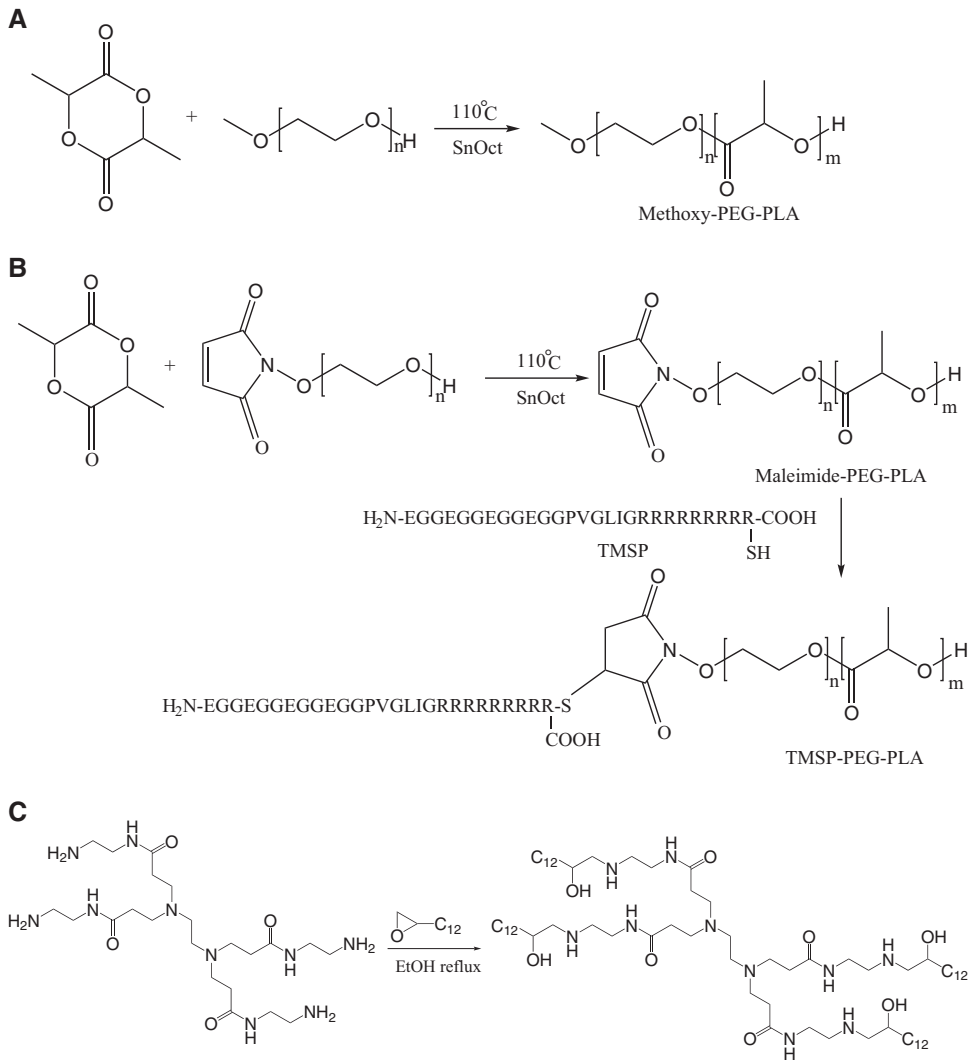

Fig. 2 Synthetic procedure of **a** PEG-PLA copolymer, **b** maleimide-PEG-PLA and TMSP-PEG-PLA, and **c** the amphiphilic dendrimer G0–G14

injection was denoted Day 0), with saline given as a control. When the tumors remained constant in size without growth, we stopped giving the drugs until relapse occurred and the tumor growth began to accelerate again. The second round of treatment was administered at Day 13 and Day 16. The tumor size was measured by calipers every 2–3 days, and tumor volume was calculated as volume = length × $(\text{width})^2/2$. At 24 h after the last intravenous injection, the mice were killed, the tumors were isolated, and a piece of tumor tissue was lysed in TRNzol A+. Then, the VEGF mRNA was extracted and analyzed by qRT–PCR as described above. To observe the microvascular density, tumors were collected and sectioned for immunohistochemical analysis against CD31.

The anti-tumor effect and safety evaluation was also conducted on HT-1080 human fibrosarcoma cell tumor models. HT-1080 cells were injected subcutaneously in the right armpit of BALB/c nu/nu mice, which were then divided randomly into 6 groups and injected with saline (Control), TMSP-ADENS/siRNA/PTX, ADENS/siRNA/PTX, TMSP-ADENS/siVEGF, TMSP-ADENS/siN.C or Taxol intravenously at Day 0, 2, 4 and 7. The doses of siRNA and PTX were 1 mg/kg and 5 mg/kg, respectively. The tumor volume and body weight were measured during treatment. Then, TMSP-ADENS/DiD (DiD = 80 μg/kg) was injected at Day 9. After 24 h, the mice were killed, and the tumors were excised, frozen in OCT embedding medium and cut into 8 μm sections. The DiD fluorescence was used to evaluate the distribution of DiD-loaded TMSP-ADENS in the different groups after treatment. Sections were also labeled and stained using a CD31 antibody (Abcam, Cambridge, USA) following the manufacturer's protocol to observe the tumor vasculature. The sections were visualized by confocal microscopy.

In vivo safety study

As a safety indicator, the body weight of all the mice was monitored during the treatment process. Peripheral blood was subjected to a blood examination with a hemocytometer, in which the RBC, WBC, PLT, GRN%, and HGB were detected and compared.

Statistical analysis

All data were presented as the means ± SD of at least three samples. Statistical significance was determined by one-way analysis of variance (ANOVA). A $P < 0.05$ is considered statistically significant ($^{*}P < 0.05$, $^{**}P < 0.01$, and $^{***}P < 0.001$).

Results and Discussion

Design and characterization of ADENS co-encapsulating siRNA and PTX

PEG-PLA, TMSP-PEG-PLA, and G0–C14 were synthesized by the procedures shown in Fig. 2. The PEG-PLA and maleimide-PEG-PLA copolymers were synthesized by ring-opening polymerization[34], and the cationic amphiphilic dendrimer termed G0–C14 was synthesized by the ring opening of 1,2-epoxytetradecane by generation 0 of the poly(amidoamine) (PAMAM) dendrimers[35]. The structures of the materials were confirmed by ^{1}H NMR (400 MHz, $CDCl_3$, Bruker Daltonics, Germany) and matrix-assisted laser desorption-ionization time of flight mass spectrometry (MALDI-TOF MS, AB SCIEX, Redwood City, USA; Figure S1, Supporting Information).

The ADENS was prepared by assembly of the amphipathic copolymer PEG-PLA and G0–C14 through a double emulsion-solvent evaporation method (Fig. 3a). TMSP-ADENS was prepared by the same procedure with 5% (mol ratio) PEG-PLA replaced by TMSP-PEG-PLA. Generation 0 of the PAMAM dendrimer was chosen for its minimal cytotoxicity and convenient synthesis compared to higher generations as well as its ability to still provide a considerable positive charge to entrap siRNA[31]. Both G0–C14 and PEG-PLA are amphiphilic polymers and thus can spontaneously self-assemble in water into spherical nanostructures[36,37]. To investigate the structural integrity of the ADENS—in other words, to confirm that the ADENS was not a simple mixture of two independent types of nanoparticles composed of G0–C14 and PEG-PLA—Förster resonance energy transfer (FRET) experiments were employed. When DiI-loaded G0–C14 nanoparticles (137.1 nm, +55.6 mV) and DiO-loaded PEG-PLA nanoparticles (145.6 nm, +2.1 mV) were mixed for 2 h at room temperature and excited at DiO's excitation wavelength of 484 nm, a decrease in the DiO emission was observed simultaneously with an increase in the DiI emission at 566 nm (Fig. 3b). As the FRET phenomenon would occur only when the distance between the fluorescence pairs was less than 10 nm, i.e., the distance that allowed energy transfer from the donor to the receptor[32,38], this indicated that the loaded compounds were close to each other due to two materials having fused together. These results suggested that the two materials had good miscibility and compatibility and that once mixed together, they had a tendency to self-assemble to form hybrid nanoparticles. This was mainly attributed to the hydrophobic interactions between the two kinds of amphiphilic polymers. As characterized by dynamic light scattering (DLS), the ADENS showed a uniform diameter of ~140 nm, while increasing the weight ratio of G0–C14 had no significant impact on the diameter but could increase the zeta potential (Fig. 3c), consistent with the positive charge of the G0–C14.

To further investigate the molecular interactions between siRNA and the cationic amphiphilic dendrimer during ADENS preparation, the localization of siRNA in the primary emulsion was investigated. As shown in Fig. 4a, almost all of the FAM-siRNA was localized in the inner water phase with a G0–C14/siRNA weight ratio of 1:1. As the weight ratio of G0–C14/siRNA increased, minimal FAM-siRNA was observed in the inner water phase, and it mainly distributed in the interphase of water and oil. When the ratio increased to 30/1, the FAM-siRNA completely colocalized with the G0–C14, contributing to the electrostatic interaction and complexation of siRNA with the positively charged materials.

In a gel retardation assay (Fig. 4b), PEG-PLA nanoparticles without G0–C14 were nearly unable to entrap siRNA even at PEG-PLA/siRNA weight ratios of 180 and 270. The incorporation of G0–C14 significantly increased the siRNA loading capacity. The migration of siRNA in agarose gel was completely retarded in the ADENS when the G0–C14/siRNA weight ratio was higher than 10/1. Therefore, the ADENS could efficiently neutralize and package siRNA.

siRNA is vulnerable to RNase in serum, so we explored the stability of siRNA in serum. The stability of siRNA in ADENS was detected using both free siRNA and PEI/siRNA as controls. The qualitative comparison images are displayed in Fig. 4c, where the free siRNA showed almost complete degradation after 3 h incubation and PEI/siRNA degraded faster than G0–C14/siRNA and ADENS/siRNA. Both G0–C14/siRNA and ADENS/siRNA still showed weak bands after 24 h of incubation. The quantification of the band intensity is shown in Figure S2.

After screening a series of formulation and preparation processes, we chose a fixed formulation of PEG-PLA: G0–C14:PTX:siRNA = 9:1:0.5:0.1 (weight ratio). The TEM images showed a coronal structure of the hydrophobic layer (Fig. 5a), and we inferred that the structure of the ADENS was a hollow core/shell spherical nanoparticle. In contrast to electrically adsorbing siRNA on the surface by simple self-assembly, the ADENS built by the

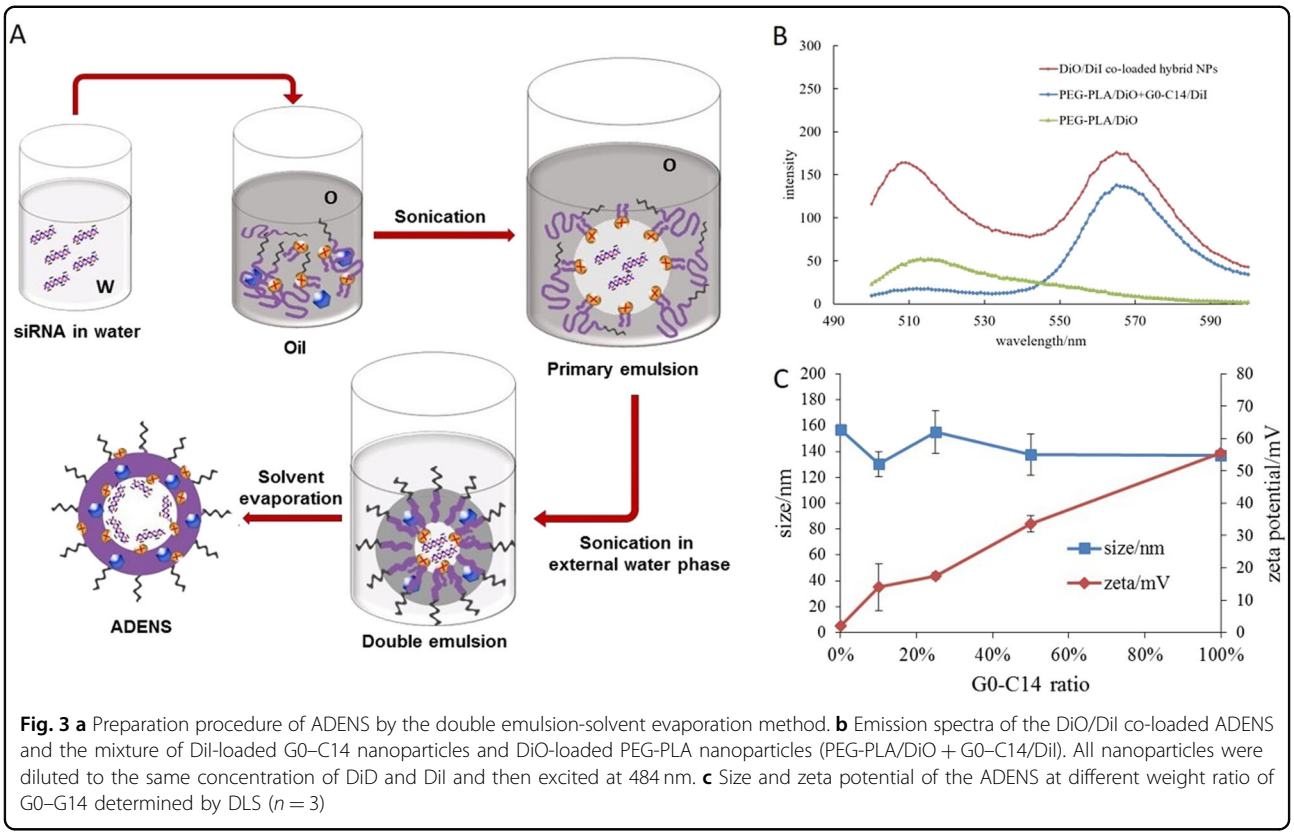

Fig. 3 a Preparation procedure of ADENS by the double emulsion-solvent evaporation method. **b** Emission spectra of the DiO/DiI co-loaded ADENS and the mixture of DiI-loaded G0–C14 nanoparticles and DiO-loaded PEG-PLA nanoparticles (PEG-PLA/DiO + G0–C14/DiI). All nanoparticles were diluted to the same concentration of DiD and DiI and then excited at 484 nm. **c** Size and zeta potential of the ADENS at different weight ratio of G0–G14 determined by DLS ($n = 3$)

double emulsion-solvent evaporation method entrapped siRNA in the hollow core with a relatively neutral PEG surface to protect siRNA from RNase in vivo[39]. The middle PLA layer allowed encapsulation of water-insoluble drugs, and the encapsulation efficiency of PTX was over 90% (Table 1). Both ADENS/siRNA/PTX and TMSP-ADENS/siRNA/PTX had similar size (~140 nm), polydispersity index (PDI) (<0.15) and zeta potential (+10 mV; Fig. 5b and Table 1). The size and PDI changes during storage at room temperature (~25 °C) were measured. The results are given in the supporting information (Figure S3) and showed that there was no change in the size and PDI after 5 days, indicating that the nanocarriers did not break in this period.

As shown by the release curve (Fig. 5c), the release of drugs from the ADENS underwent two stages. From 1 to 12 h, the drugs adsorbed by the nanocarriers were released at a relatively fast rate, and the cumulative release of PTX and siRNA was (23.5 ± 2.69)% and (15.0 ± 1.05)%, respectively. Then, the drugs encapsulated in the nanocarriers were released at a steady and slow rate based on polymer degradation and drug diffusion[16–18]. Due to the different locations of PTX and siRNA (PTX was adsorbed more on the surface, while siRNA was more wrapped in the core), as well as the diffusibility of the two drugs, PTX released slightly faster than siRNA. Therefore, the ADENS could transport the two drugs to the tumor site or tumor cells and then facilitate drug release. Prolonged drug release is crucial to ensure persistent effects[18,39].

Effects of TMSP Modification on Cellular Uptake of ADENS

Cellular internalization is crucial for siRNA and PTX to exert their effects[40]. We hoped that TMSP could be activated by MMP-2/9 to expose the CPP moiety to further improve the cellular uptake of the nanocarriers. Here, HT-1080 cells and A375 cells are selected because both are known as cell lines with high expression of MMP-2/9[41,42]. In HT-1080 cells treated with free FAM-siRNA and various FAM-siRNA-loaded nanocarriers at the same concentration for 4 h, the uptake of TMSP-ADENS was significantly higher than that of the ADENS and was even comparable to that of CPP-ADENS (CPP-modified ADENS; Fig. 6a), revealing that TMSP can be cleaved by overexpressed MMP-2/9 to expose the CPP moiety and improve the cellular uptake of the nanocarriers.

To determine whether the increase in uptake was related to MMPs, MMP-2/9 and GM6001 were pre-incubated with COU-loaded nanocarriers. In A375 cells, the uptake of COU-loaded TMSP-ADENS increased with an increase in activated MMP-2/9 and decreased to a similar level as that of the ADENS in the presence of GM6001 (Fig. 6b). The cellular uptake of COU-loaded TMSP-ADENS in presence of MMPs was even higher than that of CPP-ADENS. The reason for this may be related to the COU

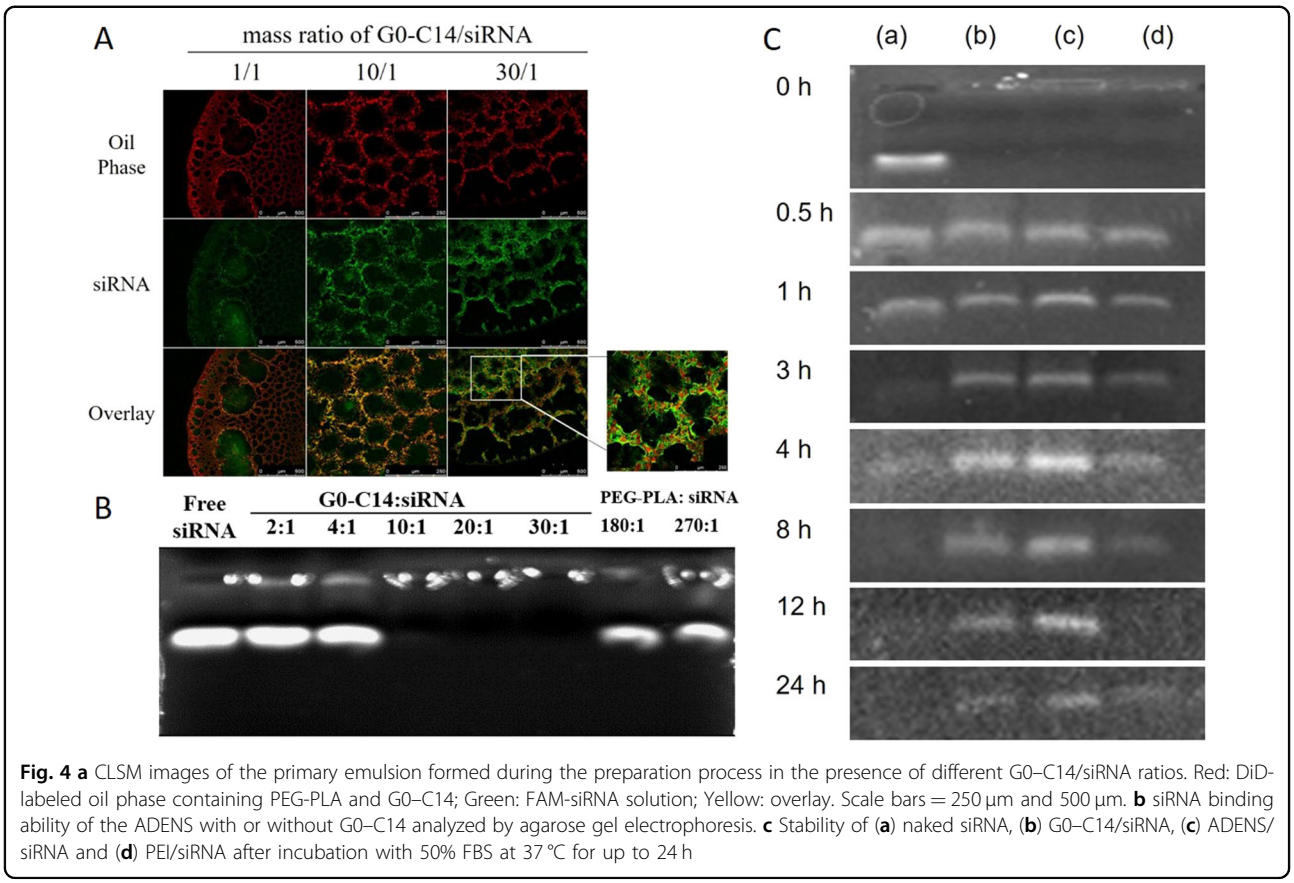

Fig. 4 a CLSM images of the primary emulsion formed during the preparation process in the presence of different G0–C14/siRNA ratios. Red: DiD-labeled oil phase containing PEG-PLA and G0–C14; Green: FAM-siRNA solution; Yellow: overlay. Scale bars = 250 μm and 500 μm. **b** siRNA binding ability of the ADENS with or without G0–C14 analyzed by agarose gel electrophoresis. **c** Stability of (**a**) naked siRNA, (**b**) G0–C14/siRNA, (**c**) ADENS/siRNA and (**d**) PEI/siRNA after incubation with 50% FBS at 37 °C for up to 24 h

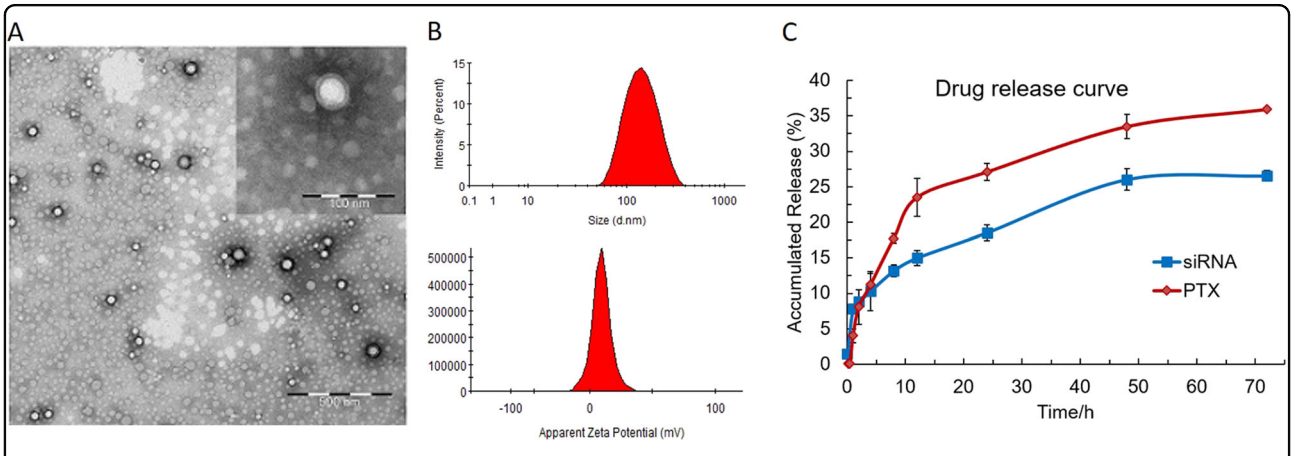

Fig. 5 a TEM image of the TMSP-ADENS containing siRNA and PTX. Scale bar = 500 nm and 100 nm (inset image). **b** Size distribution and zeta potential of the TMSP-ADENS containing siRNA and PTX. **c** siRNA and PTX release from the ADENS in PBS at pH 7.0. Data are presented as the mean ± SD ($n = 3$)

release from the nanocarriers, as unlike siRNA, COU lacked the electrostatic interaction with G0–C14. The unencapsulated COU was then quickly taken up by cells. Cellular uptake is a complex process, and further research is needed in future studies.

As a comparison, cellular uptake in PC-3 cells with low expression of MMP-2/9 was also investigated. The results revealed that the increasing rate of TMSP-ADENS/FAM-siRNA uptake in PC-3 cells was not as large as those in the other two cell lines, while superior uptake of CPP-

Table 1 Characteristics of ADENS and TMSP-ADENS

	Diameter (nm)	PDI	Zeta (mV)	E.E of PTX (%)
Blank ADENS	131.4 ± 3.67	0.147 ± 0.04	17.80 ± 7.23	/
ADENS/siRNA	140.6 ± 4.46	0.149 ± 0.03	14.85 ± 5.14	/
ADENS/siRNA/PTX	138.6 ± 9.55	0.147 ± 0.02	10.81 ± 2.08	90.97 ± 3.33
TMSP-ADENS/siRNA/PTX	140.5 ± 1.67	0.149 ± 0.01	10.53 ± 4.91	91.03 ± 4.21

[a]Data are expressed as the mean ± SD value for at least three different preparations

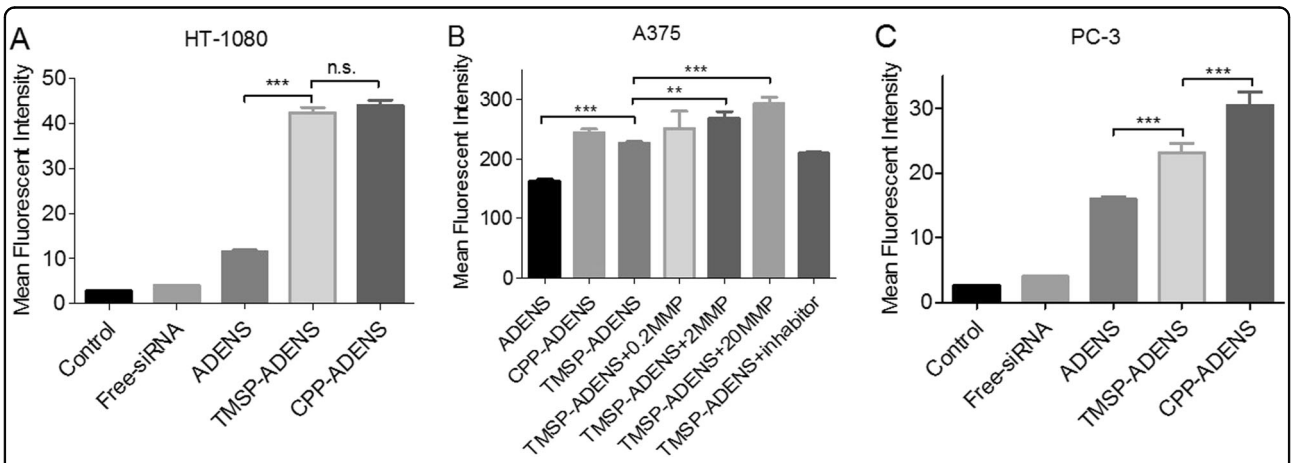

Fig. 6 Cellular uptake of various FAM-siRNA-loaded ADENS in (**a**) HT-1080 and (**c**) PC-3 cells. **b** Cellular uptake of COU-loaded TMSP-ADENS in A375 cells in the presence of GM6001 (an MMP inhibitor) and activated MMPs at different concentrations ranging from 0.2 μg/mLto 20 μg/mL. All data are presented as the mean ± SD ($n = 3$). *$P < 0.05$; **$P < 0.01$; ***$P < 0.001$; NS not significant

ADENS was observed in PC-3 cells (Fig. 6c). All these results demonstrated that the TMSP were efficient in improving the cellular uptake of the ADENS in an MMP-dependent manner. As MMPs have been identified as a characteristic of the tumor microenvironment, TMSP-ADENS should achieve tumor microenvironment-sensitive drug delivery in vivo and increase the efficiency and specificity of encapsulated drugs.

Intracellular trafficking and endosome escape of ADENS

To observe the intracellular delivery of siRNA and PTX, the double-labeled ADENS and TMSP-ADENS (FAM-siRNA and Nile Red to represent siRNA and PTX, respectively) were incubated with HT-1080 cells for 4 h and investigated by CLSM[7]. FAM-siRNA and Nile Red colocalized and were delivered simultaneously into cells by TMSP-ADENS (Fig. 7a). Consistent with the cellular uptake results by FACS (Fig. 6), TMSP-ADENS significantly increased the cellular concentration of FAM-siRNA and Nile Red after incubation for 4 h compared to the unmodified ADENS. We could also see that siRNA and Nile Red were distributed as fluorescent spots in the cytoplasm.

After being internalized, carriers must successfully achieve endosomal escape and release siRNA into the cytoplasm to realize efficient siRNA-mediated gene silencing. HT-1080 cells were transfected with FAM-siRNA-loaded TMSP-ADENS, and then the endosomes/lysosomes were stained with LysoTracker Red at 2 h, 4 h and 8 h. A relatively high colocalization (yellow) intensity of the FAM-siRNA (green) and LysoTracker Red (red) fluorescence in the cytoplasm was observed after incubation for 2 h, indicating that most TMSP-ADENS/FAM-siRNA was still trapped in endosomes in the early phase of uptake. At 4 h and 8 h, most of the green fluorescence was separated from the red fluorescence, and the fluorescence intensity did not decrease (Fig. 7b), indicating that TMSP-ADENS/FAM-siRNA had successfully escaped from the endosomes. The mechanism was that the amino-rich PAMAM part in G0–C14 had a high pH buffering capacity and could take advantage of the acidic environment inside the endosome to enhance endosomal escape by the "proton sponge" effect to disintegrate the endosomal membrane[43]. In addition, some interspersed green fluorescent particles appeared in the cytoplasm, indicating that some of the siRNA did not release from the nanocarriers. This corresponded to the sustained release of siRNA from the stable nanocarriers (Fig. 5c).

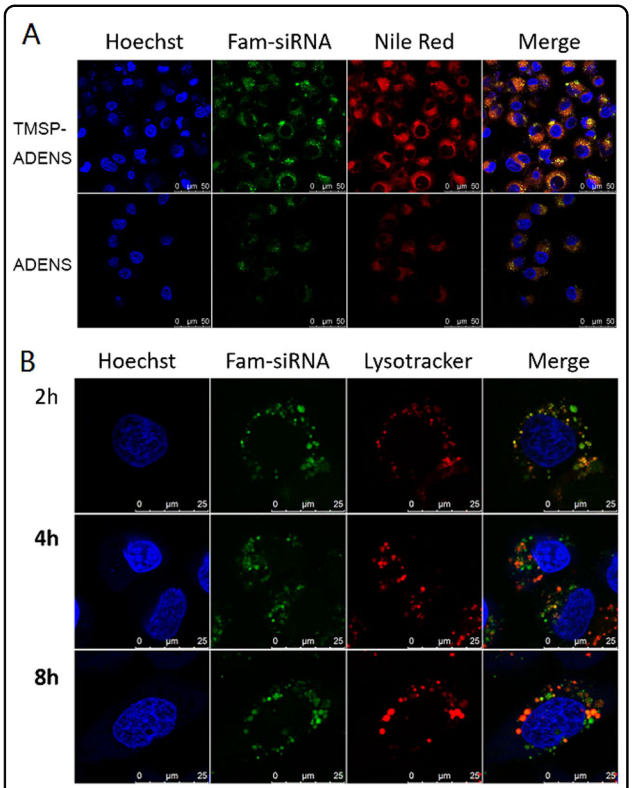

Fig. 7 a Confocal microscopy images of the intracellular distribution of TMSP-ADENS and ADENS loaded with both FAM-siRNA (green) and Nile Red (red) in HT-1080 cells after incubation for 4 h. The concentrations of FAM-siRNA and Nile Red were 100 nM and 1.25 mM, respectively. **b** Intracellular behavior of TMSP-ADENS/FAM-siRNA in HT-1080 cells after incubation for 2 h, 4 h and 8 h. Cell nuclei were stained with Hoechst 33258 (blue), and lysosomes were stained by Lysotracker Red (red in **b**)

Gene silencing in vitro

Angiogenesis is the basis of tumor growth, invasion and metastasis for almost all solid tumors, and the process is driven mainly by vascular endothelial growth factor (VEGF). Therefore, we examined whether the TMSP-ADENS encapsulating anti-VEGF siRNA could silence the VEGF gene in A375 cells. As shown in Fig. 8a, after treatment with TMSP-ADENS/siVEGF and ADENS/siVEGF (siVEGF at 100 nM), the secreted protein was reduced to lower than 20% compared to the untreated group. The VEGF mRNA suppression was determined by qRT–PCR after treatment with different formulations at the same siVEGF concentration of 50 nM (Fig. 8b), and the result showed that TMSP-ADENS/siVEGF decreased the expression of VEGF mRNA by 54.2% compared with the control, while ADENS/siVEGF reduced VEGF mRNA by 25.8%. In contrast, there was no significant protein reduction (Fig. 8a) or mRNA knockdown (Fig. 8b) in the free siRNA and siN.C treatment groups. In combination with the uptake study results, we reasonably deduced that TMSP-ADENS could improve the gene inhibition rate by promoting the cellular uptake of siRNA. In addition to silencing the endogenic VEGF gene, the silencing effect on the exogenous gene was also observed by detecting green fluorescence protein (GFP) in GFP-transfected U87 cells, and TMSP-ADENS/siGFP caused the highest inhibition rate of GFP expression (Figure S4).

The above studies proved that TMSP-ADENS was a reliable siRNA transfection system that could deliver siRNA into cells, escape from the lysosome, and then suppress target genes. The gene-silencing effect was significantly improved by TMSP modification to enhance the cellular uptake selectivity.

Antiproliferative effects of PTX-loaded ADENS

The MTT assay was performed to evaluate the cytotoxicity of blank TMSP-ADENS, ADENS/PTX, TMSP-ADENS/PTX and Taxol in HT-1080, PC-3, and A375 cells (Fig. 9). After incubation for 48 h, TMSP-ADENS/PTX exhibited stronger growth inhibition effects on the three cells than ADENS/PTX. TMSP-ADENS/PTX exerted an antiproliferative effect on A375 cells similar to Taxol, whereas it was not as lethal as Taxol in HT-1080 and PC-3 cells. These results were possibly related to the different expression levels of MMPs and different sensitivity of those cells[44,45]. The more drugs the cells took up, the better the antiproliferative effects were. No significant cytotoxicity was observed in blank TMSP-ADENS alone, proving that the materials were biocompatibility and safe for drug delivery.

ADENS biodistribution in the xenograft model

The biodistribution of the injected ADENS/Cy5-siRNA and TMSP-ADENS/Cy5-siRNA was further investigated in the HT-1080 mice xenograft model using near-infrared fluorescence imaging. The background fluorescence in the nude mice was very weak and showed no significant effect on the experiment (Figure S5). TMSP-ADENS/Cy5-siRNA showed stronger tumor accumulation than ADENS/Cy5-siRNA, especially at 11 h and 24 h (Fig. 10), indicating that TMSP modification improved accumulation and significantly prolonged the probe retention time in the tumor. This was expected to correspond to the MMP-triggered activation and the enhanced cellular uptake and penetration effect of CPP. TMSP-modified nanoparticles preferentially accumulated in and penetrated the tumor, indicating that it would have strong anti-angiogenic and anti-tumor effects.

Accumulation of the ADENS in tumor

The spatial and temporal distribution of drugs in tumor tissue is an important factor in determining tumor response to therapies. Penetration and accumulation of the ADENS in tumors were tested by labeling ADENS and

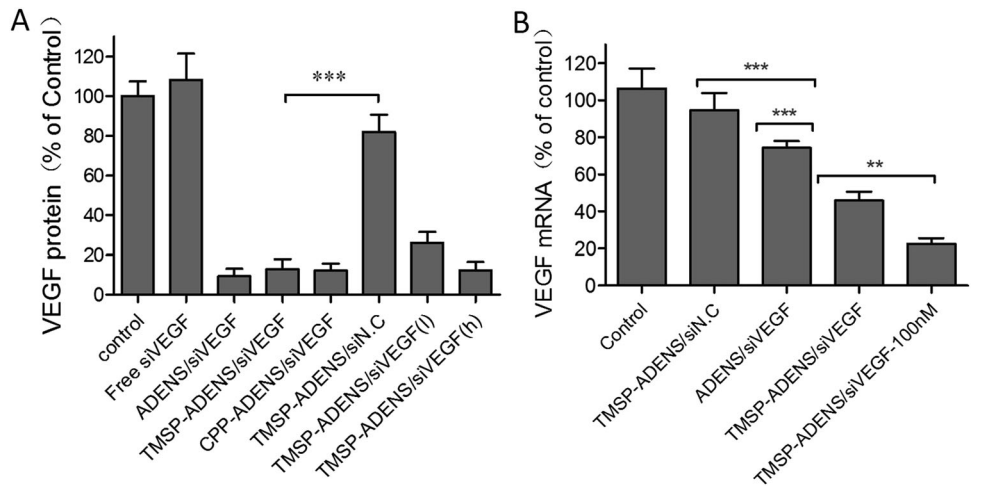

Fig. 8 In vitro VEGF gene-silencing efficiency of TMSP-ADENS. a VEGF protein expression in A375 cells determined by ELISA after culturing with various formulations. The unspecified concentrations of siVEGF and siN.C were 100 nM, whereas (*l*) and (*h*) denote a low concentration of 50 nM and a high concentration of 150 nM, respectively. **b** VEGF mRNA in A375 cells determined by qRT–PCR after culturing with various formulations. The unspecified concentrations of siVEGF and siN.C were 50 nM. All data are presented as the mean ± SD ($n = 3$),*$P < 0.05$, **$P < 0.01$, ***$P < 0.001$

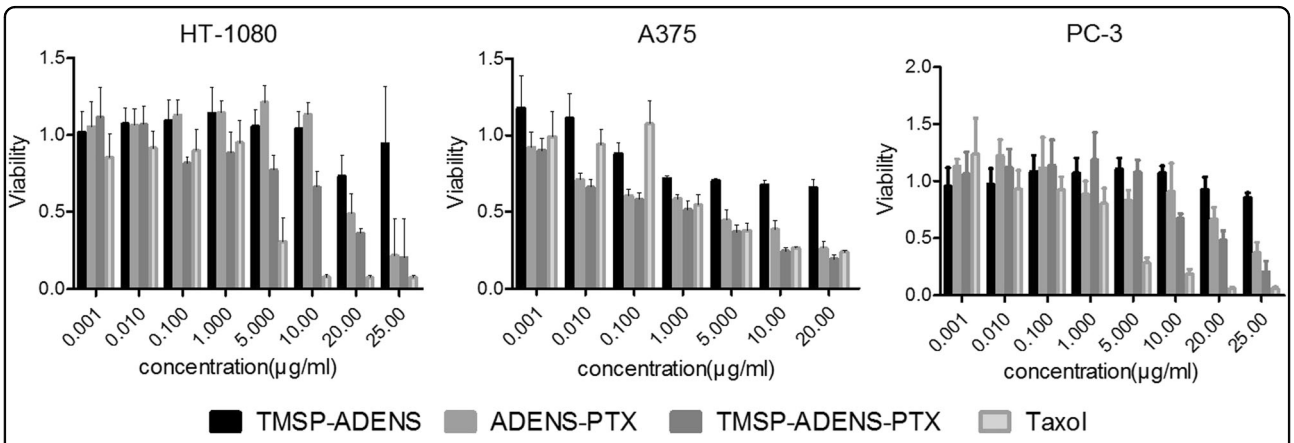

Fig. 9 The cell viability of HT-1080, A375 and PC-3 cells cultured with various PTX-loaded ADENS and Taxol at the same PTX dose and the corresponding blank TMSP-ADENS after 48 h. All data are presented as the mean ± SD ($n = 6$)

TMSP-ADENS with the fluorescent dye DiD to monitor them in HT-1080 cells xenograft mice model. Tumors were removed at 24 h post-injection. As observed by CLSM of frozen sections, more TMSP-ADENS was observed in tumor tissues than ADENS (Fig. 11). In accordance with the near-infrared fluorescence imaging results (Fig. 10), there was more accumulation of TMSP-ADENS in the tumor site due to the tumor-specific property of TMSP, as TMSP could identify the characteristics of the tumor microenvironment and CPP could be activated by MMP-2/9, thus improving cellular internalization and tumor penetration. In contrast, unmodified nanoparticles accumulated in the tumor via a non-specific mechanism, mainly by the EPR effect. Therefore, TMSP modification successfully improved the tumor targeting of the ADENS.

Anti-tumor effects in A375 cell-xenografted mice

Human melanoma is a highly aggressive cancer with poor prognosis and high secretion of VEGF, which mediates angiogenesis for further progress and metastasis. Here, we developed a tumorigenesis-relapse model to assess the inhibitory effects of VEGF gene-silencing siRNA together with PTX co-delivered by TMSP-ADENS on A375 tumor growth, invasion and relapse. As shown in Fig. 12a, after two drug administrations at the early stage of tumorigenesis, the tumors nearly stopped growing with no significant changes in volume, and this period lasted for 11 days. Then,

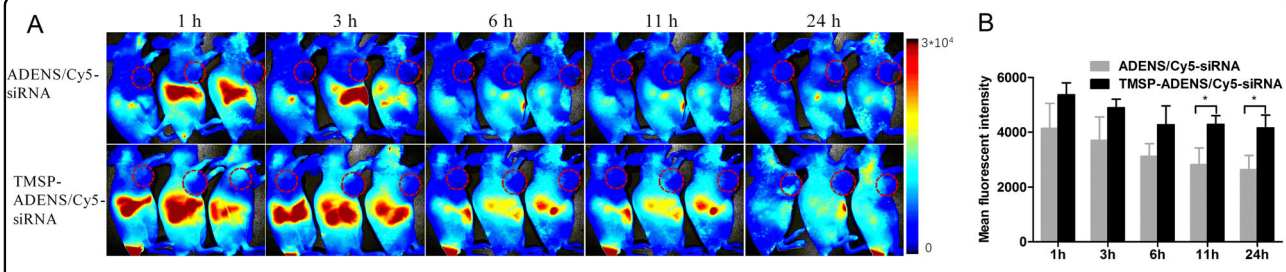

Fig. 10 In vivo biodistribution of the ADENS in HT-1080 tumor-bearing nu/nu mice visualized by NIR imaging. Fluorescent images at the indicated time points after intravenous administration of ADENS/Cy5-siRNA and TMSP-ADENS/Cy5-siRNA (**a**) and quantification of the mean fluorescent intensity (**b**). The red dotted circles are the location of the tumors. All data are presented as the mean ± SD ($n = 3$), $^*P < 0.05$

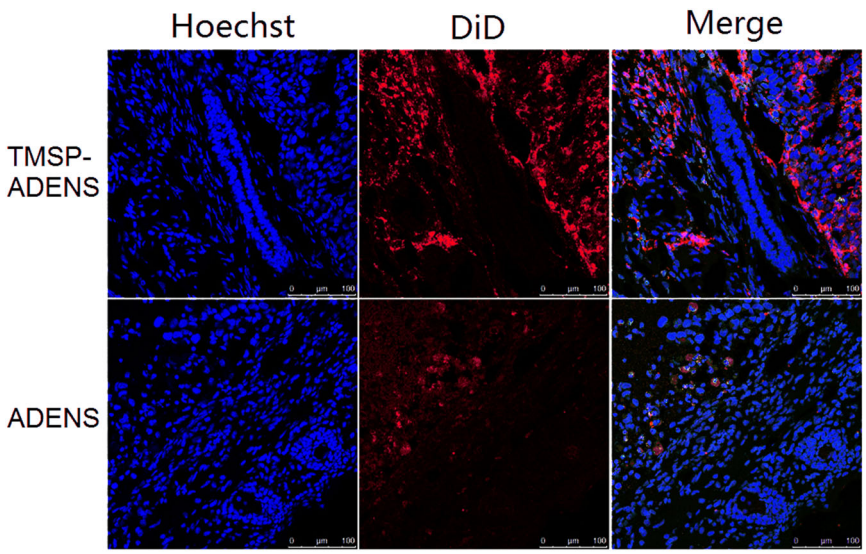

Fig. 11 Distribution of the TMSP-ADENS and ADENS in tumor tissue observed by CLSM images in HT-1080 tumor-bearing mice after i.v. injection. The nanocarriers were labeled with DiD (Red), and the cell nuclei were stained with Hoechst 33258 (Blue). (Scale bar, 100 μm)

the groups given saline, TMSP-ADENS/siN.C and Taxol showed an abrupt acceleration in tumor growth. This change was considered a sign of tumor relapse, and thus, we begun to administer the therapies again at Day 13 and 16. By the 23th day, the tumor volume of the control group given saline had increased nearly 20 times and still exhibited a rapid growth tendency. The effect of Taxol at the administered dose became very weak; in fact the tumor shrunk immediately after injection but began to grow rapidly once the drug was removed. Moreover, Taxol administration could no longer inhibit tumor growth when the tumor relapsed. Interestingly, the groups given ADENS/siRNA/PTX and TMSP-ADENS/siRNA/PTX still did not show significant change in tumor volume. The TMSP-ADENS/siRNA/PTX-treated group showed the lowest tumor growth rate and best anti-relapse effect at the end of the observation with the tumors remaining almost unchanged. The group also showed the highest survival rate (Fig. 12b). We could see that co-delivery of PTX and siVEGF in TMSP-ADENS had considerable benefits in terms of inhibiting tumor growth at a relatively low dose. The superior anti-tumor effect involved the effects of both PTX and the anti-angiogenic therapy. The drugs delivered by TMSP-ADENS distributed more in the tumor (Fig. 10) and better accessed the tumor cells (Fig. 11) by both the EPR effect and the tumor microenvironment-triggered cell penetration enhancement[24]. Furthermore, once arriving at tumor cells, the ADENS could sustainably release the drugs, whereas free drugs would be quickly eliminated from the body. All these effects together led to the outstanding therapeutic efficacy shown by TMSP-ADENS.

In vivo VEGF gene silencing

VEGF mRNA expression was detected by qRT–PCR to evaluate whether the siRNA delivered by TMSP-ADENS could cause VEGF gene silencing in vivo. The results

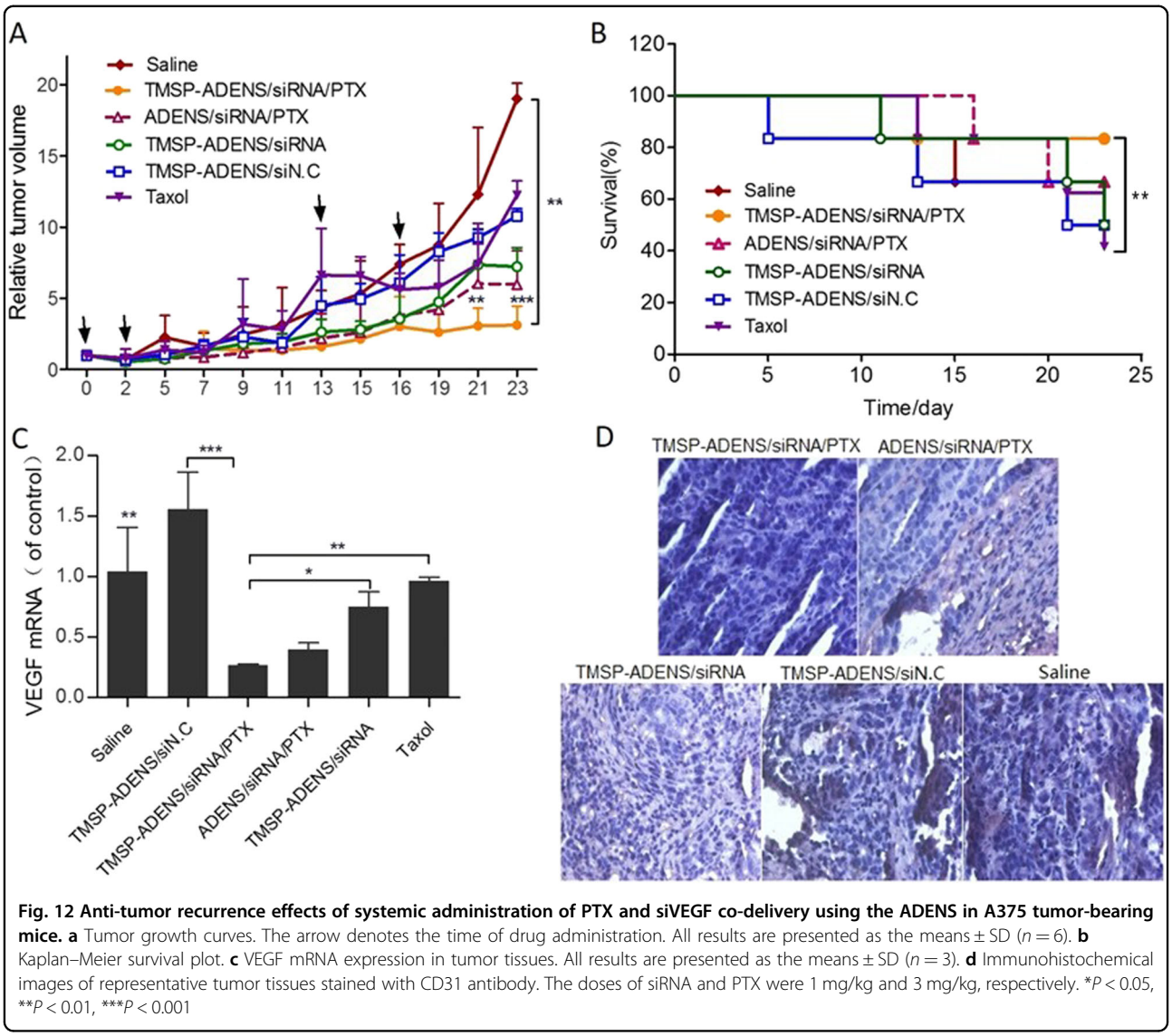

Fig. 12 Anti-tumor recurrence effects of systemic administration of PTX and siVEGF co-delivery using the ADENS in A375 tumor-bearing mice. a Tumor growth curves. The arrow denotes the time of drug administration. All results are presented as the means ± SD ($n = 6$). **b** Kaplan–Meier survival plot. **c** VEGF mRNA expression in tumor tissues. All results are presented as the means ± SD ($n = 3$). **d** Immunohistochemical images of representative tumor tissues stained with CD31 antibody. The doses of siRNA and PTX were 1 mg/kg and 3 mg/kg, respectively. $^{*}P < 0.05$, $^{**}P < 0.01$, $^{***}P < 0.001$

revealed that TMSP-ADENS/siRNA/PTX inhibited VEGF mRNA expression by 73% (Fig. 12c), the highest inhibition rate among all groups. VEGF is the most important regulator of tumor angiogenesis and mediates a series of endothelial cell activities and formation of abnormal tumor vessels. For tumor vasculature detection, immunohistochemical analysis of tumor sections was performed using an antibody against CD31, a specific marker of endothelial cells[7]. As indicated in Fig. 12d, the CD31-positive signals in brown could be seen in the TMSP-ADENS/siN.C and saline groups, indicating the formation of tumor angiogenesis. In contrast, in the groups given VEGF siRNA, the positive signals significantly decreased. These results revealed that VEGF siRNA could efficiently play an RNA interference role in vivo when co-delivered with PTX by TMSP-ADENS. As reported before, tumor vessels are fundamental for delivering nutrients for tumor growth and metastasis to distant organs, and the abnormal vasculature, together with the resulting abnormal microenvironment, forms a tough barrier for the delivery of cancer therapy[46]. Regulating tumor vascularization by inhibiting VEGF is a valid method for cancer therapy.

Anti-tumor effect and safety evaluation in HT-1080 tumor models

To verify the broad capability of TMSP-ADENS/siRNA/PTX in cancer therapy, the anti-tumor effect was also investigated in human fibrosarcoma HT-1080 tumor models. Compared with the saline control, TMSP-ADENS/siRNA/PTX showed stronger tumor growth inhibition (Fig. 13a, b), whereas TMSP-ADENS/siN.C had almost no effect. Immunofluorescence staining against CD31 confirmed the reduction in tumor angiogenesis. As shown in Fig. 13c, the green fluorescence signals

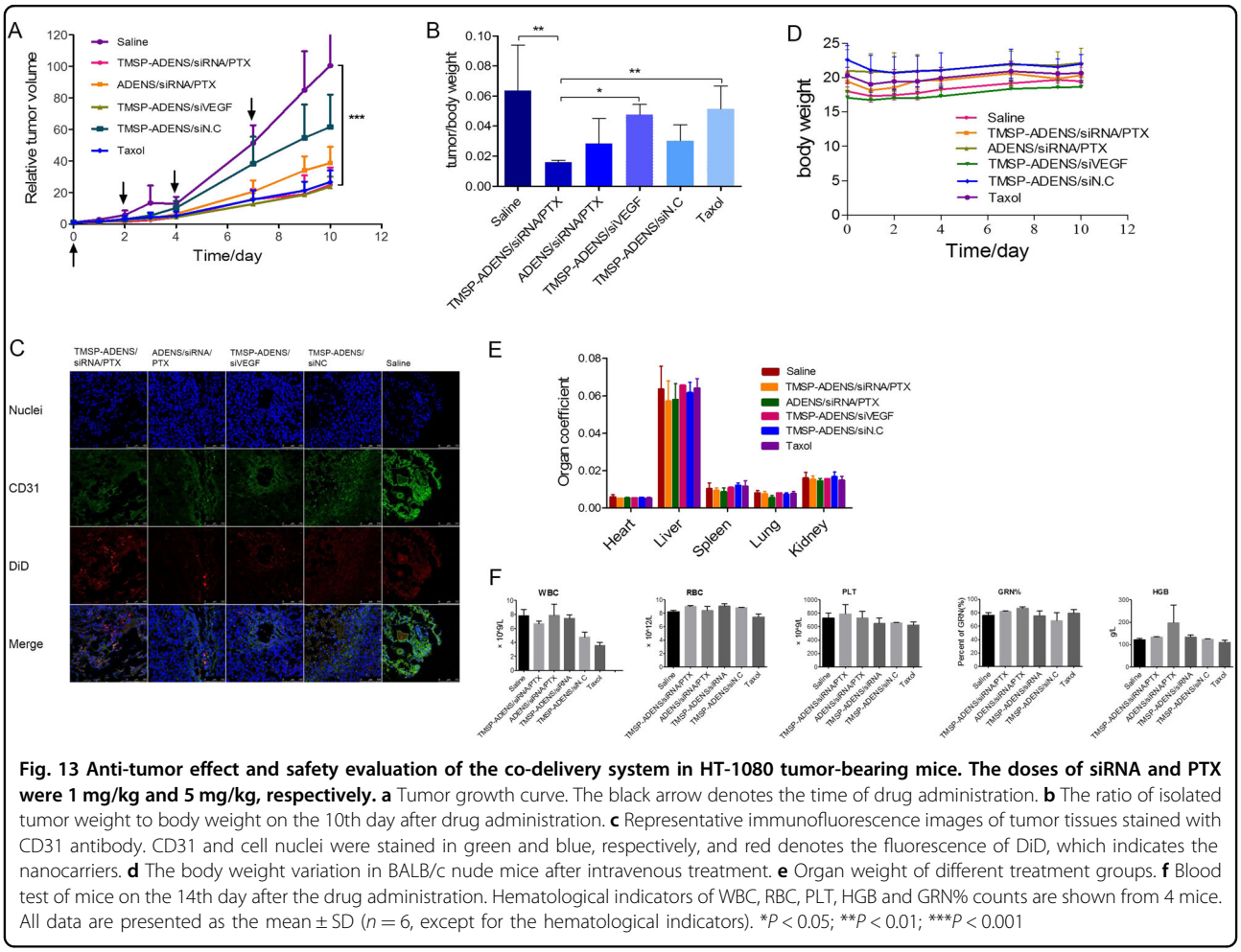

Fig. 13 Anti-tumor effect and safety evaluation of the co-delivery system in HT-1080 tumor-bearing mice. The doses of siRNA and PTX were 1 mg/kg and 5 mg/kg, respectively. a Tumor growth curve. The black arrow denotes the time of drug administration. **b** The ratio of isolated tumor weight to body weight on the 10th day after drug administration. **c** Representative immunofluorescence images of tumor tissues stained with CD31 antibody. CD31 and cell nuclei were stained in green and blue, respectively, and red denotes the fluorescence of DiD, which indicates the nanocarriers. **d** The body weight variation in BALB/c nude mice after intravenous treatment. **e** Organ weight of different treatment groups. **f** Blood test of mice on the 14th day after the drug administration. Hematological indicators of WBC, RBC, PLT, HGB and GRN% counts are shown from 4 mice. All data are presented as the mean ± SD ($n = 6$, except for the hematological indicators). $^{*}P < 0.05$; $^{**}P < 0.01$; $^{***}P < 0.001$

representing CD31-positive tumor vessels were abundant among the tumors in the saline group, and a large proportion of the drugs (DiD-labeled nanocarriers, red) were trapped in the vessels without access to tumor cells, which may severely limit their therapeutic efficacy. In contrast, only a small amount of CD31-positive signal was detected in the TMSP-ADENS/siRNA/PTX group, and the drugs spread among the tumor tissue. All these results revealed the outstanding anti-tumor effect of co-delivery using TMSP-ADENS.

Safety is an essential factor that is as crucial as efficacy in assessing drug therapies because severe side effects caused by chemotherapeutics is a big limitation on their clinical applications. One goal of combining siRNA and chemotherapeutic agents in one delivery vehicle is to reduce the drug dose and non-specific distribution, thereby decreasing the toxicity and other side effects. In consideration of safety, the body weight change, hematologic indicators and organ index after different treatments were monitored. The mice body weight did not decrease during the treatment (Fig. 13d), and the organ coefficient (organ weight/body weight) showed no difference among these groups (Fig. 13e). The levels of WBC, RBC, PLT and other indicators did not change significantly compared with each control group ($P > 0.05$) after three drug injections (Fig. 13f). We also analyzed the histopathology of the lung, and no obvious changes were observed (Figure S6). In fact, we could reasonably conclude that the TMSP-ADENS co-delivery system was safe at the test dose for in vivo administration and that it caused no noticeable loss of weight, aberrance in hematologic indicators or damage to organs.

Conclusions

In this study, we developed an amphiphilic dendrimer (G0–C14) engineered PEG-PLA nanoparticle for the systemic and simultaneous co-delivery of siRNAs and PTX. The ADENS exhibited a unique hollow core/shell structure with appropriate size and potential, and the structure offered multiple functions. It was capable of encapsulating both liposoluble PTX and hydrosoluble siRNA in different sections with high encapsulation

efficiency. The TMSP-modified ADENS showed enhanced cellular uptake, tumor penetration and accumulation compared to ADENS via an MMP-2/9-triggered mechanism. After arriving at the tumor site, TMSP-ADENS sustainably released PTX and siRNA to ensure persistent drug activity. By prolonging the effects of cell apoptosis induction and target VEGF gene silencing to suppress tumor angiogenesis, the co-delivery system inhibited tumor growth and relapse while also reducing the toxicity arising from high-dose chemotherapeutics and siRNAs. TMSP-ADENS provided a potential strategy for effective co-delivery of siRNA and PTX for anti-tumor treatment in a synergistic manner.

Acknowledgements
We acknowledge the National Nature Science Foundation of China (No. 81673365, No. 81473156) and the National Key Basic Research Program (No. 2013CB932501) for their funding of this work.

Conflict of interest
The authors declare that they have no conflict of interest.

Supplementary information accompanies this paper at https://doi.org/10.1038/s41427-018-0027-4.

Received: 6 June 2017 Revised: 7 December 2017 Accepted: 10 December 2017.
Published online: 12 April 2018

References

1. Saraswathy, M. & Gong, S. Q. Recent developments in the co-delivery of siRNA and small molecule anticancer drugs for cancer treatment. *Mater. Today* **17**, 298–306 (2014).
2. Lage, H. An overview of cancer multidrug resistance: a still unsolved problem. *Cell Mol. Life Sci.* **65**, 3145–3167 (2008).
3. Li, Y., Wang, J., Wientjes, M. G. & Au, J. L. Delivery of nanomedicines to extracellular and intracellular compartments of a solid tumor. *Adv. Drug. Deliv. Rev.* **64**, 29–39 (2012).
4. Creixell, M. & Peppas, N. A. Co-delivery of siRNA and therapeutic agents using nanocarriers to overcome cancer resistance. *Nano Today* **7**, 367–379 (2012).
5. Zhang, J. et al. Synergistic anti-tumor effects of combined gemcitabine and cisplatin nanoparticles in a stroma-rich bladder carcinoma model. *J. Control Release* **182**, 90–96 (2014).
6. Dong, D. W. et al. pH-responsive complexes using prefunctionalized polymers for synchronous delivery of doxorubicin and siRNA to cancer cells. *Biomaterials* **34**, 4849–4859 (2013).
7. Yang, Z. Z., Li, J. Q., Wang, Z. Z., Dong, D. W. & Qi, X. R. Tumor-targeting dual peptides-modified cationic liposomes for delivery of siRNA and docetaxel to gliomas. *Biomaterials* **35**, 5226–5239 (2014).
8. Dong, D. W., Gao, W., Liu, Y. J. & Qi, X. R. Therapeutic potential of targeted multifunctional nanocomplex co-delivery of siRNA and low-dose doxorubicin in breast cancer. *Cancer Lett.* **359**, 178–186 (2015).
9. Resnier, P., Montier, T., Mathieu, V., Benoit, J. P. & Passirani, C. A review of the current status of siRNA nanomedicines in the treatment of cancer. *Biomaterials* **34**, 6429–6443 (2013).
10. Oh, Y. K. & Park, T. G. siRNA delivery systems for cancer treatment. *Adv. Drug Deliv. Rev.* **61**, 850–862 (2009).
11. Shi, J., Xiao, Z., Votruba, A. R., Vilos, C. & Farokhzad, O. C. Differentially charged hollow core/shell lipid-polymer-lipid hybrid nanoparticles for small interfering RNA delivery. *Angew. Chem. Int. Ed.* **50**, 7027–7031 (2011).
12. Tseng, Y. C., Mozumdar, S. & Huang, L. Lipid-based systemic delivery of siRNA. *Adv. Drug Deliv. Rev.* **61**, 721–731 (2009).
13. Davis, M. E. The first targeted delivery of siRNA in humans via a self-assembling, cyclodextrin polymer-based nanoparticle: from concept to clinic. *Mol. Pharm.* **6**, 659–668 (2009).
14. Musacchio, T., Vaze, O., D'souza, G. & Torchilin, V. P. Effective stabilization and delivery of siRNA: reversible siRNA–phospholipid conjugate in nanosized mixed polymeric micelles. *Bioconjug. Chem.* **21**, 1530–1536 (2010).
15. Tyler, B., Gullotti, D., Mangraviti, A., Utsuki, T. & Brem, H. Polylactic acid (PLA) controlled delivery carriers for biomedical applications. *Adv. Drug Deliv. Rev.* **107**, 163–175 (2016).
16. Li, Y., Qi, X. R., Maitani, Y. & Nagai, T. PEG-PLA diblock copolymer micelle-like nanoparticles as all-trans-retinoic acid carrier: *in vitro* and *in vivo* characterizations. *Nanotechnology* **20**, 055106 (2009).
17. Feng, L. et al. Pharmaceutical and immunological evaluation of a single-dose hepatitis B vaccine using PLGA microspheres. *J. Control Release* **112**, 35–42 (2006).
18. Lobovkina, T. et al. In vivo sustained release of siRNA from solid lipid nanoparticles. *Acs Nano* **5**, 9977–9983 (2011).
19. Cho, H., Gao, J. & Kwon, G. S. PEG-b-PLA micelles and PLGA-b-PEG-b-PLGA sol-gels for drug delivery. *J. Control Release* **240**, 191–201 (2016).
20. Ahn, H. K. et al. A phase II trial of Cremorphor EL-free paclitaxel (Genexol-PM) and gemcitabine in patients with advanced non-small cell lung cancer. *Cancer Chemother. Pharmacol.* **74**, 277–282 (2014).
21. Mandal, B., Mittal, N. K., Balabathula, P., Thoma, L. A. & Wood, G. C. Development and *in vitro* evaluation of core-shell type lipid-polymer hybrid nanoparticles for the delivery of erlotinib in non-small cell lung cancer. *Eur. J. Pharm. Sci.* **81**, 162–171 (2016).
22. Mandal, B. et al. Core-shell-type lipid-polymer hybrid nanoparticles as a drug delivery platform. *Nanomedicine* **9**, 474–491 (2013).
23. Hadinoto, K., Sundaresan, A. & Cheow, W. S. Lipid–polymer hybrid nanoparticles as a new generation therapeutic delivery platform: A review. *Eur. J. Pharm. Biopharm.* **85**, 427–443 (2013).
24. Gao, W., Xiang, B., Meng, T. T., Liu, F. & Qi, X. R. Chemotherapeutic drug delivery to cancer cells using a combination of folate targeting and tumor microenvironment-sensitive polypeptides. *Biomaterials* **34**, 4137–4149 (2013).
25. Gao, W. et al. Targeting and microenvironment-responsive lipid nanocarrier for the enhancement of tumor cell recognition and therapeutic efficiency. *Adv. Healthc. Mater.* **4**, 748–759 (2015).
26. Shi, N. Q., Qi, X. R., Xiang, B. & Zhang, Y. A survey on "Trojan Horse" peptides: opportunities, issues and controlled entry to "Troy". *J. Control Release* **194**, 53–70 (2014).
27. Cerrato, C. P., Lehto, T. & Langel, U. Peptide-based vectors: recent developments. *Biomol. Concepts* **5**, 479–488 (2014).
28. Shi, N. Q., Gao, W., Xiang, B. & Qi, X. R. Enhancing cellular uptake of activable cell-penetrating peptide-doxorubicin conjugate by enzymatic cleavage. *Int. J. Nanomed.* **7**, 1613–1621 (2012).
29. Xiang, B. et al. PSA-responsive and PSMA-mediated multifunctional liposomes for targeted therapy of prostate cancer. *Biomaterials* **34**, 6976–6991 (2013).
30. Shi, N. Q. & Qi, X. R. Taming the wildness of "Trojan-Horse" peptides by charge-guided masking and protease-triggered demasking for the controlled delivery of antitumor agents. *Acs Appl. Mater. Inter* **9**, 10519–10529 (2017).
31. Khan, O. F. et al. Ionizable amphiphilic dendrimer-based nanomaterials with alkyl-chain-substituted amines for tunable siRNA delivery to the liver endothelium*in vivo*. *Angew. Chem. Int. Ed.* **53**, 14397–14401 (2014).
32. Wang, A. T., Liang, D. S., Liu, Y. J. & Qi, X. R. Roles of ligand and TPGS of micelles in regulating internalization, penetration and accumulation against sensitive or resistant tumor and therapy for multidrug resistant tumors. *Biomaterials* **53**, 160–172 (2015).
33. Bawadi, H. A., Antunes, T. M., Shih, F. & Losso, J. N. In vitro inhibition of the activation of Pro-matrix Metalloproteinase 1 (Pro-MMP-1) and Pro-matrix metalloproteinase 9 (Pro-MMP-9) by rice and soybean Bowman-Birk inhibitors. *J. Agr. Food Chem.* **52**, 4730–4736 (2004).
34. Olivier, J. C., Huertas, R., Lee, H. J., Calon, F. & Pardridge, W. M. Synthesis of pegylated immunonanoparticles. *Pharm. Res.* **19**, 1137–1143 (2002).
35. Shi, J. et al. Hybrid lipid-polymer nanoparticles for sustained siRNA delivery and gene silencing. *Nanomedicine* **10**, 897–900 (2014).

36. Liu, X. X. et al. Adaptive amphiphilic dendrimer-based nanoassemblies as robust and versatile siRNA delivery systems. *Angew. Chem. Int. Ed.* **53**, 11822–11827 (2014).
37. Percec, V. et al. Self-assembly of Janus dendrimers into uniform dendrimersomes and other complex architectures. *Science* **328**, 1009–1014 (2010).
38. Gibot, L. et al. Polymeric micelles encapsulating photosensitizer: structure/photodynamic therapy efficiency relation. *Biomacromolecules* **15**, 1443–1455 (2014).
39. Zhao, J. & Feng, S. S. Nanocarriers for delivery of siRNA and co-delivery of siRNA and other therapeutic agents. *Nanomedicine* **10**, 2199–2228 (2015).
40. Zhu, X. et al. Long-circulating siRNA nanoparticles for validating Prohibitin1-targeted non-small cell lung cancer treatment. *Proc. Natl Acad. Sci. USA* **112**, 7779–7784 (2015).
41. Giambernardi, T. A. et al. Overview of matrix metalloproteinase expression in cultured human cells. *Matrix Biol.* **16**, 483–496 (1998).
42. Kryza, D. et al. Ex vivo and in vivo imaging and biodistribution of aptamers targeting the human matrix metalloprotease-9 in melanomas. *PLoS ONE* **11**, e0149387 (2016).
43. Ma, D. Enhancing endosomal escape for nanoparticle mediated siRNA delivery. *Nanoscale* **6**, 6415–6425 (2014).
44. Ma, D. X., Shi, N. Q. & Qi, X. R. Distinct transduction modes of arginine-rich cell-penetrating peptides for cargo delivery into tumor cells. *Int. J. Pharm.* **419**, 200–208 (2011).
45. Ma, D. X. & Qi, X. R. Comparison of mechanisms and cellular uptake of cell-penetrating peptide on different cell lines. *Yao Xue Xue Bao* **45**, 1165–1169 (2010).
46. Jain, R. K. Normalization of tumor vasculature: an emerging concept in anti-angiogenic therapy. *Science* **307**, 58–62 (2005).